

This manuscript has not been peer reviewed and is a preprint only. It has been submitted to the Journal of Sedimentary Research.

1

2 **The Influence of Grain Shape and Size on the Relationship Between** 3 **Porosity and Permeability in Sandstone**

4 Ryan L. Payton^{1,*}, Domenico Chiarella¹ and Andrew Kingdon²

5 ¹Clastic Sedimentology Investigation (CSI), Royal Holloway, University of London, Department
6 of Earth Sciences, Egham, Surrey, United Kingdom

7 ²British Geological Survey, Keyworth, Nottingham, United Kingdom

8 * Corresponding author: ryan.payton.2015@live.rhul.ac.uk

9

10 Twitter Handles:

11 RLP: @RyanLPayton

12 DC: @nocode_dc

13 AK: @AndyGeology

14 CSI: @CSI_RHUL

15 RHUL Earth Sciences: @RHULEarthSci

16

17 This manuscript has been submitted for publication in the Journal of Sedimentary Research.

18 Please note that this manuscript has not undergone peer review and is yet to be formally
19 accepted for publication. Subsequent versions of the manuscript may have different content.

20 If accepted the final version of this manuscript will be available via the 'Peer-reviewed
21 Publication DOI' link on this webpage. Please feel free to contact any of the authors, we
22 welcome any feedback.

This manuscript has not been peer reviewed and is a preprint only. It has been submitted to the Journal of Sedimentary Research.

23

ABSTRACT

24

An accurate and reliable description of the relationship between porosity and permeability in geological materials is valuable in understanding subsurface fluid movement.

25

26

This is of great importance for studies of reservoir characterisation, useful for energy

27

exploitation, carbon capture, use and storage (CCUS) and groundwater contamination and

28

remediation. Whilst the relationship between pore characteristics and porosity and

29

permeability are well examined, there is scope for further investigation into the influence of

30

grain characteristics on porosity and permeability due to the inherent relationship between

31

grains and related pores. In this work we use digital image analysis (DIA) of reconstructed 3D

32

X-ray micro computed tomographic (μ CT) images to measure porosity, permeability and

33

segment individual grains enabling the measurement of grain shape (sphericity) and size

34

(Ferret diameter). We compare two marker-based watershed workflows to grain boundary

35

segmentation before applying the most reliable one to our images. We found there to be a

36

positive relationship between grain sphericity and porosity according to $\phi = 1.22\phi_s - 0.42$

37

whereas no such relationship exists with grain size. We applied our grain shape and size

38

measurements to calculate a Kozeny-Carman (K-C) porosity-permeability fit which was found

39

to be unsatisfactory, possibly due to significant deviation from the K-C assumption that grains

40

are spherical. Therefore, we show that a simpler fit of the form $K = 10^{5.54} \phi^{3.7}$, excluding

41

any influence of grain characteristics, is most suitable for the studied materials and that grain

42

shape and size is not influential on the porosity-permeability relationship in a K-C paradigm.

43

44

INTRODUCTION

45

The relationship between porosity and permeability is very significant for reservoir

46

characterisation studies applied to energy exploitation, carbon storage and aquifer

This manuscript has not been peer reviewed and is a preprint only. It has been submitted to the Journal of Sedimentary Research.

47 contamination and remediation. Constraining the relationship between these two important
48 reservoir parameters is beneficial as measurement of porosity alone can then be used to
49 predict permeability, which is typically expensive and time consuming to measure both
50 physically in a lab and computationally using digital image analysis (DIA). Furthermore,
51 permeability can only be measured directly in the lab on small scale samples or in the field at
52 the macro scale using pump tests, producing two results which often do not closely agree.
53 Therefore, identification of a reliable and accurate relationship between porosity and
54 permeability using computed tomography (CT) imaging could have far-reaching implications
55 for reconciling this issue.

56

57 *Modelling a Porosity-Permeability Relationship*

58 The Kozeny-Carman (K-C) relationship, proposed by Kozeny (1927) and later modified
59 by Carman (1937), is a simple yet broadly effective and widely used (Mavko and Nur 1997; de
60 Lima and Sri Niwas 2000; Urumovic and Urumovic Sr. 2014; Berg 2014; Hommel et al. 2018)
61 technique of relating porosity to permeability. Bear (1972) suggested a modification to the K-
62 C equation which allows grain diameter to be employed as a component which influences the
63 permeability. Additionally, Hommel et al. (2018) show that an additional grain sphericity term
64 may also be used. Whilst a K-C-based approach is successful in many instances, its accuracy
65 may be questioned when applied to materials which possess a significant proportion of grains
66 which deviate substantially from being spherical. The limitation of a K-C approach is that
67 grains are considered spherical and packed in a regular arrangement; allowing pores to be
68 considered as capillary bundles. The inherent relationship between the pore structure and
69 the grains which create the pore space indicates that a detailed investigation of grain

This manuscript has not been peer reviewed and is a preprint only. It has been submitted to the Journal of Sedimentary Research.

70 characteristics is of utmost importance in understanding the porosity-permeability
71 relationship.

72 In this work we aim to investigate whether the inclusion of grain sphericity and 3D
73 Feret diameter (referred to herein as grain size) in a K-C paradigm facilitates a better quality
74 fit to the relationship between porosity and permeability. We compare our modified K-C
75 approach to a simpler fit using porosity and permeability measurements alone, excluding any
76 influence of grain shape or size. To do so, the individual relationships between porosity and
77 permeability and grain sphericity and size are investigated and considered in light of the
78 concept of grain anisotropy, as introduced by Nabawy (2014).

79

80 *A Methodology for Making Digital 3D Grain Measurements*

81 Whilst grain size and shape measurement has traditionally been done manually using
82 callipers and sieve analysis (W. D. Keller 1945; Schäfer and Teyssen 1987; Wang et al. 2013;
83 Suhr et al. 2018) we have used digital image analysis (DIA) to segment individual grains in 3D
84 using reconstructed X-ray micro computed tomographic (μ CT) image stacks of each sample.
85 μ CT imaging has been used in a wide variety of fields related to geosciences since its rise in
86 popularity as a non-destructive and high resolution image acquisition technique (Blunt et al.
87 2013; Bultreys et al. 2015; Thomson et al. 2018, 2020b; Payton et al. 2021). When paired with
88 DIA, large amounts of quantitative and visually useful data may be obtained. Unlike when
89 using optical imaging, X-ray imaging is dependent primarily on phase density therefore, grain
90 boundaries are difficult to identify, particularly in a tightly packed sandstone.

91 In this work we discuss and investigate grain segmentation using two relatively simple
92 marker-based watershed workflows. Watershed algorithms, established by Beucher & Meyer
93 (2018), split a phase up into individual components by treating the image as a topographic

This manuscript has not been peer reviewed and is a preprint only. It has been submitted to the Journal of Sedimentary Research.

94 surface, identifying topographic lows and assigning a seed point to each. Flooding from each
95 seed point allows digital watersheds to be identified and are used to define the boundaries
96 between individual features (Sun et al. 2019). The challenge arises from making correct
97 identification of marker points so as not to have multiple grains sharing one marker
98 (undersegmentation) or the opposite where multiple markers are assigned to a single grain
99 (oversegmentation). Techniques such as the bring up (Kong and Fonseca 2018; Leonti et al.
100 2020) and bring down (Shi and Yan 2015; Sun et al. 2019) methods have been developed to
101 try and tackle this issue but can often be computationally demanding and may still produce
102 inaccuracies.

103 Segmentation of the solid phase alone allows identification of individual grains which
104 can then be measured digitally in 3D. Segmentation is arguably the most important and
105 usually most difficult process in DIA (Campbell et al. 2018) given that poor segmentation will
106 directly result in poor and likely misleading results. It is notoriously difficult to segment
107 features within a given phase which are touching, consequently many techniques have been
108 developed to tackle this challenge, often providing unique solutions to a given sample set or
109 type of sample (shelly, angular, rounded, etc...) (Campbell et al. 2018; Kong and Fonseca 2018;
110 Furat et al. 2019; Leonti et al. 2020) as there is not a one size fits all solution (Campbell et al.
111 2018).

112 We assess two segmentation workflows and use the most effective to analyse a
113 collection of 22 sandstone samples from three different geological formations (i.e., Wilmslow
114 Sandstone Formation, Sellafeld, UK; Brae Formation Sandstone, Miller Field, North Sea, UK;
115 Minard Formation Sandstone, Porcupine Basin, North Atlantic Ocean). Finally, we use the
116 grain measurements alongside digital measurements of porosity and permeability to

This manuscript has not been peer reviewed and is a preprint only. It has been submitted to the Journal of Sedimentary Research.

117 investigate the quality of a K-C-based fit to the porosity-permeability relationship using grain
118 shape and size inputs.

119

120

METHODS

121 A variety of sandstone samples have been selected from several different reservoir
122 units which host significant levels of porosity. Samples from the Wilmslow Sandstone
123 Formation (Sellafield, UK; Payton et al. 2021), Brae Formation Sandstone (North Sea, UK;
124 Thomson et al. 2020b) and the Porcupine Basin (North Atlantic Ocean) were acquired and
125 imaged at the London Natural History Museum Imaging and Analysis Centre. Table 1
126 summarises the materials used in this work and specifies the associated literature detailing
127 initial sample imaging where relevant. We chose to exclude samples which exhibited no
128 connected porosity and therefore no permeability for the purpose of this study.

129 The material pertaining to the Porcupine Basin was collected and prepared using the
130 same technique outlined by Thomson et al. (2020b) and Payton et al. (2021). From each
131 sample a mini plug measuring 5 mm in diameter and 10 mm in length was cut and imaged
132 using X-ray micro computed tomography (μ CT), detailed by Payton et al. (2021). For further
133 information about the voxel size and subsampled volume of each sample we refer the reader
134 to the Supplementary Information.

135

136

Image Processing

137 The acquired μ CT image stacks of each sample underwent pre-processing using the
138 commercial software package PerGeos (v1.7.0). From each image stack a sub-volume was
139 extracted to remove external voxels and any image slices which contained significant beam
140 hardening artefacts. In order to aid the segmentation process we employed a non-local means

This manuscript has not been peer reviewed and is a preprint only. It has been submitted to the Journal of Sedimentary Research.

141 filter which enhances the contrast between greyscale phases and removes speckled noise
142 throughout the images (Buades et al. 2008, 2010).

143

144 *Porosity and Permeability*

145 We followed the method detailed by Payton et al. (2021) to measure porosity and
146 permeability - a brief outline is described here. We made use of the well-known automatic
147 binary segmentation algorithm designed by Otsu (1979) to separate and label the solid grain
148 phase and pore space. In some cases, it was necessary to constrain the greyscale range over
149 which the algorithm was allowed to operate on where exceedingly bright phases were
150 present which meant darker grains and darker pore space were not automatically separated.

151 The volume fraction of the segmented pore space can be measured which equates to
152 the total sample porosity. We then applied the 'axis connectivity' tool along each axis in turn
153 to determine the proportion of porosity which is entirely connected between all faces of the
154 sample. We took this value to represent the connected porosity.

155 Finally, we employed the 'absolute permeability simulation' tool to run a finite
156 difference numerical simulation, solving the Stokes flow equations:

$$\nabla \mathbf{u} = 0 \quad (1)$$

$$-\nabla P + \mu \nabla^2 \mathbf{u} = 0 \quad (2)$$

157 where \mathbf{u} is velocity, P is pressure, μ is fluid viscosity equal to 1×10^{-3} Pa s for water. We
158 used an error tolerance of 10^{-6} for the convergence of the L_2 norm of the residuals as
159 recommended by Thomson et al. (2019) whilst the boundary conditions used are discussed in
160 detail by Thomson et al. (2018). The solution is a velocity field which allows for a permeability
161 value to be determined through application of Darcy's Law. Further details on this technique
162 can be found in Thomson et al. (2020b) and Payton et al. (2021).

163

164

Pore Geometry

165

166

167

168

169

170

171

172

Grain Segmentation

173

174

175

176

177

178

179

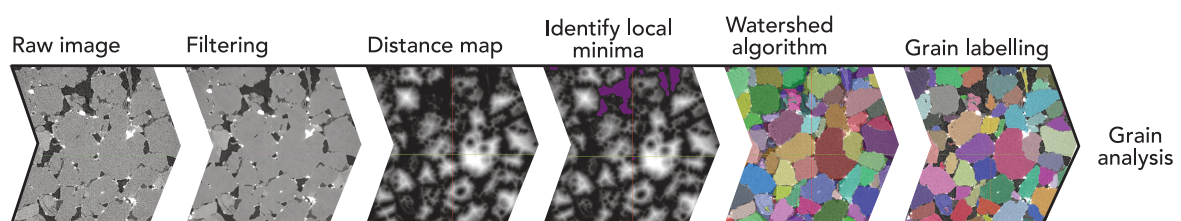
180

181

182

In order to characterise the individual pores which make up the pore structure we employed a pore network model (PNM). PNM are simplified representations of complex pore geometries using balls to represent pores and sticks to represent throats. We created PNM of the connected porosity following the methodology detailed in Payton et al. (2021) and references therein. Each PNM may be interrogated to provide information about each pore including radius and coordination number, and each throat including radius and length.

Segmentation of individual features in μ CT images has traditionally been performed using the marker-based watershed approach detailed by Beucher & Meyer (2018). This technique has been widely used in a variety of fields (Barraud 2006; Cristoforetti et al. 2008; Veta et al. 2011; Huang et al. 2018; Xue et al. 2021) to identify and split individual features in digital images. The general steps in using a watershed algorithm are shown in Figure 1 (for a more detailed description of how a watershed algorithm operates we refer the reader to Kong & Fonseca (2018) and Sun et al. (2019)). We chose to follow the workflow of watershed segmentation of grains described by Fei & Narsilio (2020) which is shown to be successful in separating grains in a variety of different sand samples which bare some resemblance to the materials investigated here.



183

Figure 1

This manuscript has not been peer reviewed and is a preprint only. It has been submitted to the Journal of Sedimentary Research.

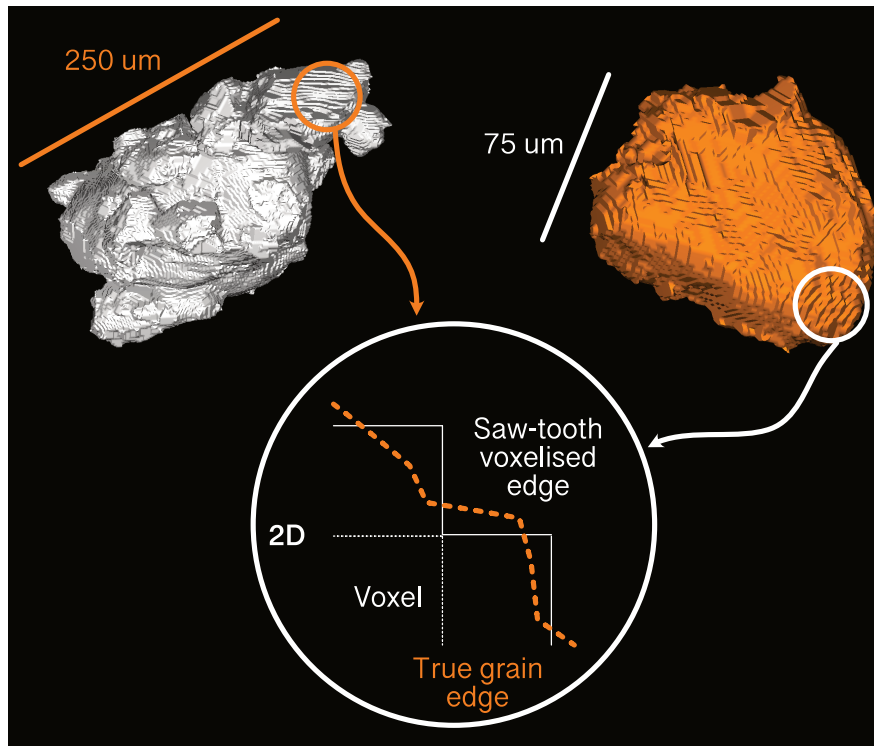
184 The method described by Fei & Narsilio (2020) uses the software package Fiji
185 (Schindelin et al. 2012) to carry out cropping and filtering. A non-local means filter is used in
186 combination with a median filter prior to using the MorphoLibJ plug-in for Fiji (Legland et al.
187 2016) which encompasses generation of a distance map and identification of seed points for
188 watershed flooding as described in Figure 1.

189

190

Grain Measurements

191 Once the watershed algorithm has run, the individual grains are labelled before the
192 Feret diameter and sphericity of each grain is measured using the 3D ImageJ Suite plug-in
193 (Ollion et al. 2013). When extracting 3D grains from μ CT images, which are voxelised, the
194 edges exhibit a saw-tooth pattern (Fig. 2). This can lead to overestimation of surface area and
195 consequently underestimation of sphericity, as detailed by (Fei et al. 2019). Therefore, we
196 acknowledge that our sphericity measurements are conservative but as the saw-tooth
197 pattern effect is present for all grains measured, the results we present are still directly
198 comparable between each other.



199 **Figure 2**

200 Whilst smoothing algorithms can be applied to reduce this effect, determining
201 appropriate parameters for such algorithms becomes heavily subjective and can cause
202 undesirable deformation of the individual grains such as volume loss. Moreover, using the
203 same degree of smoothing on a very small and a very large grain will have different impacts
204 on the resulting shape. Consequently, we chose to omit the use of any smoothing tools prior
205 to our measurements being made.

206 The automated nature of the MorphoLibJ and 3D Suite plug-ins enables this analysis
207 to be carried out simply as well as rapidly with low computational cost. Sphericity is measured
208 between 0 and 1 where 1 represents a perfect sphere. We used Feret diameter as the
209 representative grain size for all statistical analyses in this work. Some of the grain size analyses
210 performed use phi (ϕ) units, calculated from grain size values in millimetres according to:

$$\phi = -\log_2 D \quad (3)$$

This manuscript has not been peer reviewed and is a preprint only. It has been submitted to the Journal of Sedimentary Research.

211 where D is the grain diameter. We calculated the graphic mean grain size (M_z) after Folk
212 (1980) according to the following formula:

$$M_z = \frac{(\phi_{16} + \phi_{50} + \phi_{84})}{3}, \quad (4)$$

213 where ϕ_{84} represents the ϕ value at the 84th percentile. We calculated the 'inclusive graphic
214 standard deviation' introduced by Folk (1980) to determine the sorting (ϕ_1) of our samples
215 using the following formula:

$$\phi_1 = \frac{\phi_{84} - \phi_{16}}{4} + \frac{\phi_{95} - \phi_5}{6.6}. \quad (5)$$

216 We then classified the sorting of our samples following the accompanying scheme defined by
217 Folk (1980) where a smaller ϕ_1 value is representative of better sorting.

218

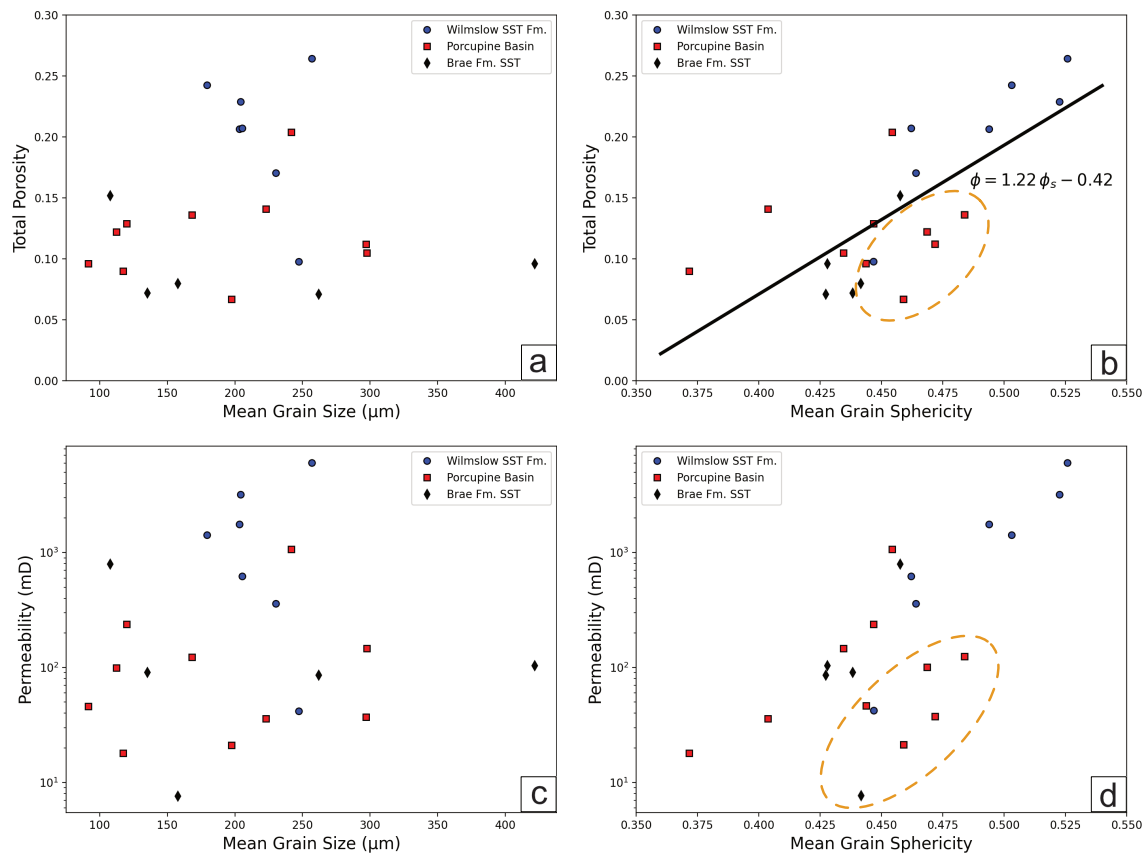
219 RESULTS

220 *Application of the Proposed Methodology*

221 Each study sample was analysed in terms of grain characteristics and the results are
222 reported in Table 2. The accompanying porosity and permeability results are reported in Table
223 3, measured in this article and by Thomson et al. (2020b) and Payton et al. (2021). Figure 3
224 shows the relationships among mean grain size, mean grain sphericity, porosity, and
225 permeability. No clear relationship between grain size and sample porosity or permeability is
226 observed (Figs. 3a and 3c). Despite this, we see a much clearer positive correlation between
227 the grain sphericity and porosity and permeability (Figs. 3b and 3d). This suggests that the
228 shape or anisotropy of the grains has a direct influence on the pore structure whereas the
229 size of the grains does not. Figure 3d highlights a collection of seven outliers showing the
230 same relationship but offset from the dominant trend between mean grain sphericity and
231 permeability. The same collection of data points is highlighted in Figure 3b, plotting mean

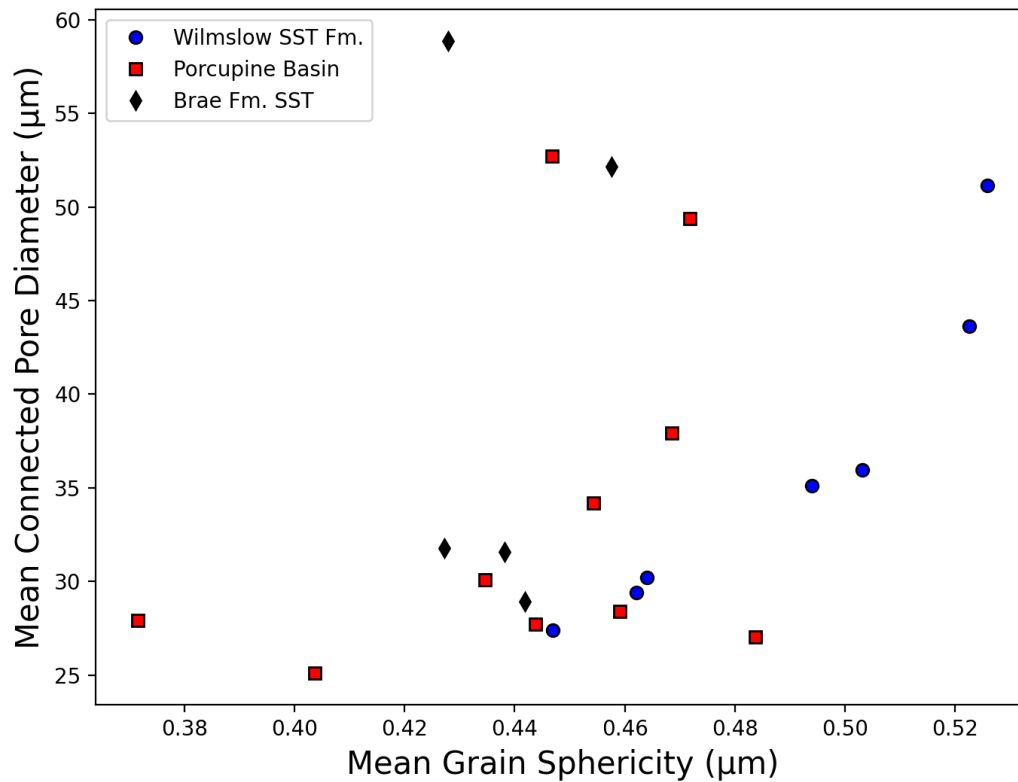
This manuscript has not been peer reviewed and is a preprint only. It has been submitted to the Journal of Sedimentary Research.

232 grain sphericity against total porosity, where they are not obviously misaligned with the rest
233 of the data points. This indicates that these apparent outliers, in the case of permeability,
234 result from a characteristic of the sample which is independent of porosity but not
235 permeability.



236 **Figure 3**

237 As the intergranular porosity is fundamentally governed by the grains themselves, we
238 investigated the relationship between the pore structure and grain sphericity. Figure 4 shows
239 a generally positive relationship between grain sphericity and the connected pore diameter
240 except for four apparent outliers across all three sample suites. Of these four outliers, two
241 belong to the group of seven identified in Figure 3d and two do not. However, the cause for
242 the occurrence of these four outliers is unclear and it seems that there is no correlation
243 between these four outliers and other measured factors such as sorting and grain size.



244 **Figure 4**

245 *Impact of Grain Shape on the Porosity-Permeability Relationship*

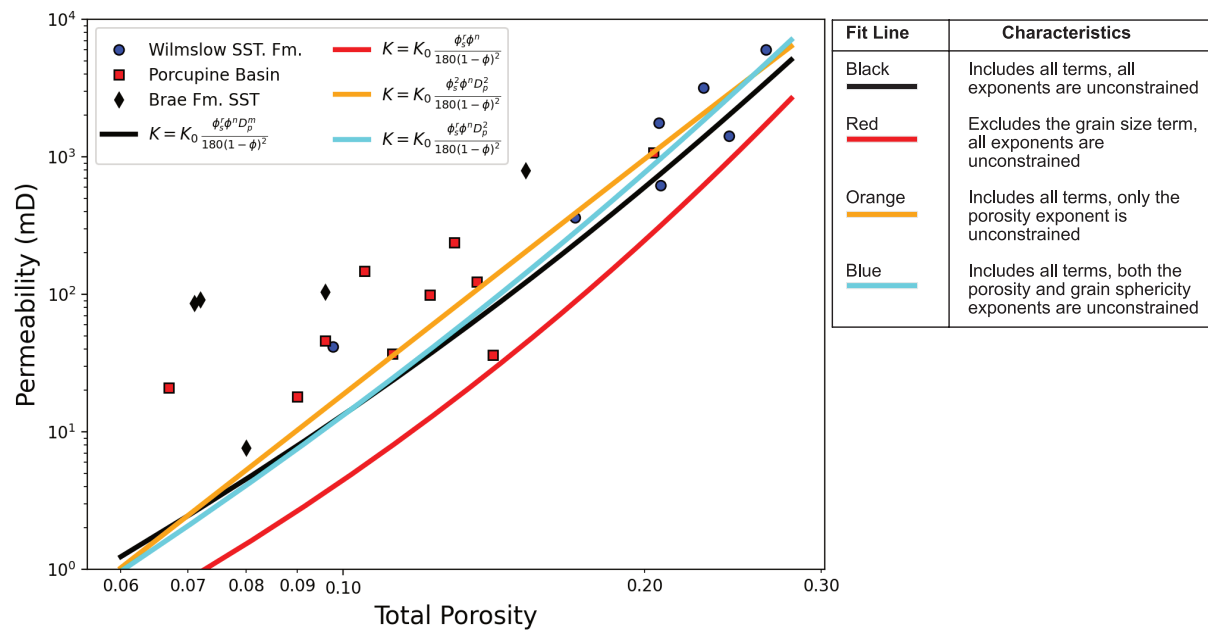
246 Our results show that the shape of the grains in a sample has an impact on the porosity
 247 and permeability. Therefore, it is reasonable to assume that the porosity-permeability
 248 relationship could be better constrained through incorporating the grain shape into the fit
 249 equation. Accordingly, we employed a modified Kozeny-Carman equation discussed by
 250 Hommel et al. (2018),

$$K = K_0 \frac{\phi_s^r \phi^n D_p^m}{180 (1 - \phi)^2}, \quad (6)$$

251 which incorporates the grain sphericity, ϕ_s and size, D_p alongside porosity, ϕ and a
 252 permeability constant, K_0 to calculate a porosity-permeability fit. We imposed a variety of
 253 constraints on the fit with regards to the three constant exponents: n , m and r , applicable to

This manuscript has not been peer reviewed and is a preprint only. It has been submitted to the Journal of Sedimentary Research.

254 porosity, grain size and grain sphericity respectively (Fig. 5), to determine the best fit with the
 255 lowest root mean square error (RMSE).

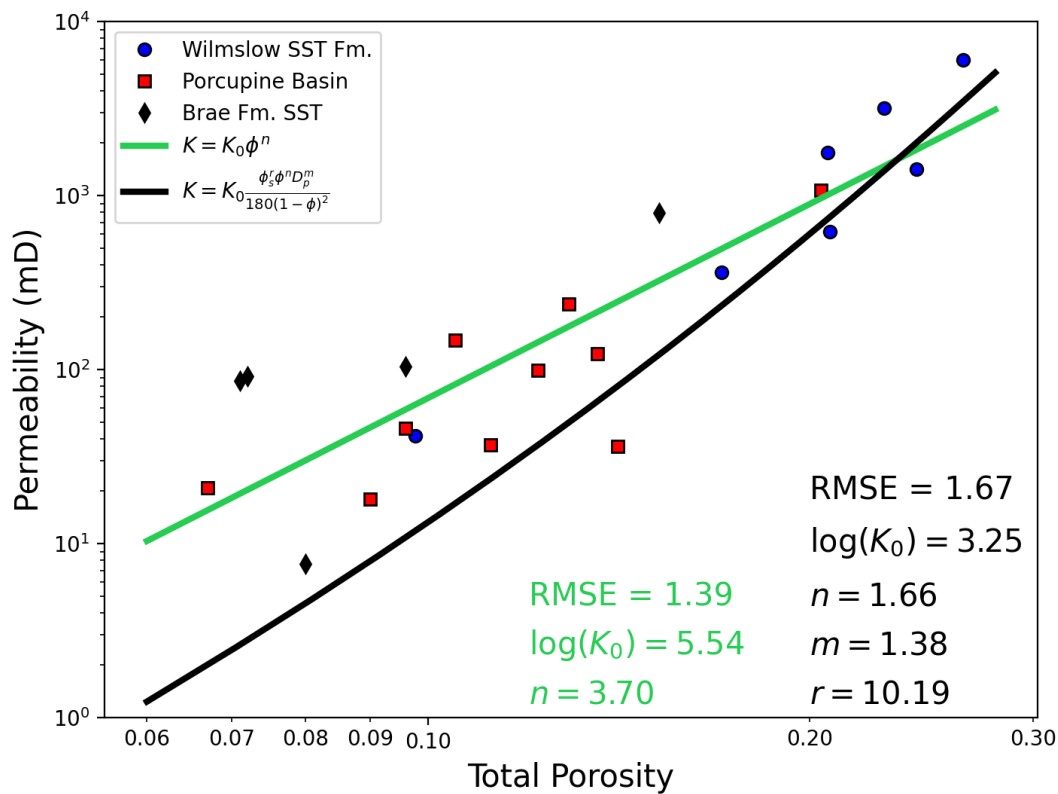


256 **Figure 5**

257 The best of the four fits based on the RMSE (Fig. 5) is the case where each exponent
 258 can vary and is not constrained in any way, shown by the black fit line. The red fit line, which
 259 omits the grain size term, produces the poorest quality fit even though we identified grain
 260 size to have no relationship with porosity or permeability (see Figs. 3a and 3c). The remaining
 261 two fit lines in cyan and orange offer fits with RMSE values just larger and therefore less
 262 successful than the black fit. The cyan and orange fits offer varying constraint on the
 263 exponents of grain size alone and grain size alongside grain sphericity respectively but
 264 importantly, both include the grain size term. Inclusion of this term, whether its exponent
 265 may vary or not, clearly allows the given fit to be of a greater quality than omitting it all
 266 together.

267 It is apparent that even the best fit achieved, shown by the black line in Figure 5, does
 268 not fit all data points effectively, especially below a total porosity of ca. 15%. Consequently,
 269 we show an additional, simpler fit which does not consider any grain characteristics in Figure

270 6 (green line) alongside the best fit identified in Figure 5. Our results show that the simpler fit
 271 which considers porosity and permeability alone is more effective, exhibiting a lower RMSE
 272 of 1.39 as opposed to 1.67 in the case of the fit incorporating the grain characteristics.



273 **Figure 6**

274

DISCUSSION

275

Grain Boundary Watershed Segmentation

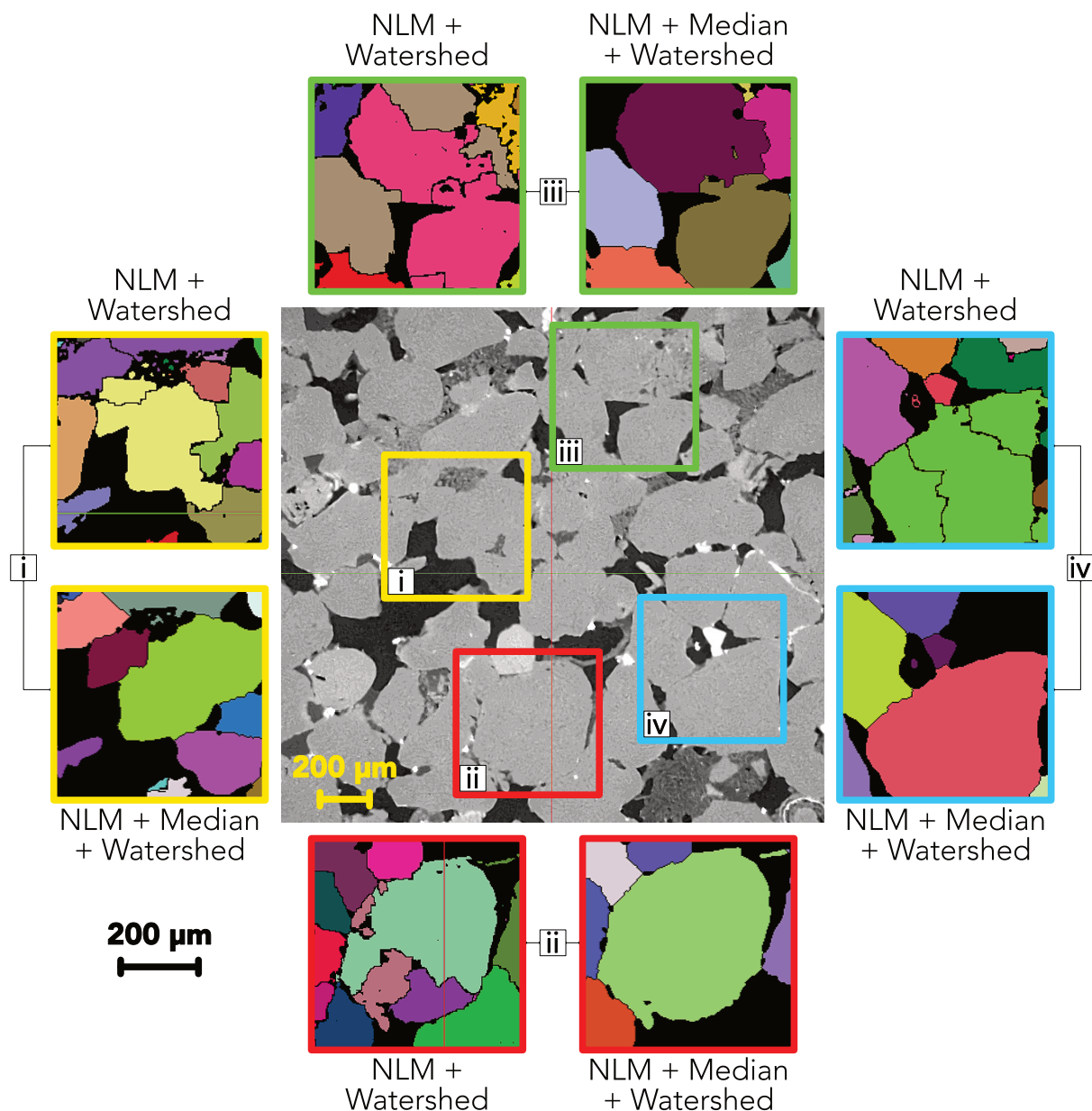
276

277 Whilst the approach that we take to segment individual grains (Fei and Narsilio 2020)
 278 is relatively straightforward, we acknowledge that there are a number of other algorithms
 279 which aim to improve the accuracy of the traditional watershed algorithm. In particular,
 280 oversegmentation is an issue, particularly when segmenting features of a wide range of sizes
 281 and shapes where multiple markers are placed within one feature (Kong and Fonseca 2018;

This manuscript has not been peer reviewed and is a preprint only. It has been submitted to the Journal of Sedimentary Research.

282 Sun et al. 2019; Leonti et al. 2020). Modified watershed approaches have been developed
283 using the bring down method (Shi and Yan 2015) and the bring up method (Kong and Fonseca
284 2018; Leonti et al. 2020) to accurately label features and their boundaries. Due to the high
285 accuracy of results reported by Fei & Narsilio (2020), the ease of implementation and minimal
286 computational cost we chose to use the traditional watershed technique with a non-local
287 means and median filter in line with the methodology described by the authors.

288 The technique used here is very similar to that applied by Thomson, et al. (2020a).
289 Thomson, et al. (2020a) implement a traditional watershed algorithm but only use a non-local
290 means filter without a median filter. The non-local means filter performs the bulk of the
291 denoising in the images very effectively, but this type of filter is not optimal for retaining or
292 improving feature boundaries. In contrast, the median filter is very effective for this purpose,
293 enhancing the clarity of feature boundaries whilst smoothing any remaining noise in the
294 images. We show the similarities and differences in the results of watershed segmentation
295 using the two approaches in Figure 7.



296 **Figure 7**

297 Our results show that the approach used by Thomson, et al. (2020a) results in some
298 oversegmentation of grains when comparing the watershed result to the greyscale CT image.
299 In contrast the approach used in this study does not show severe oversegmentation of the
300 same grains, owing to the boundary enhancement provided by the median filter.
301 Furthermore, by using the 3D Suite plug-in for Fiji, grains which are touching the boundaries
302 of the study volume can be excluded from measurement to ensure only grains which are
303 complete and truly representative are included. This was not included in the method used by

This manuscript has not been peer reviewed and is a preprint only. It has been submitted to the Journal of Sedimentary Research.

304 Thomson, et al. (2020a) and therefore partial grains may have significantly influenced the
305 mean grain measurements made.

306 Finally, Thomson, et al. (2020a) acknowledge in their work that the separated grains
307 in their work displayed an unexpected group of grains with Feret diameters of $< 63 \mu\text{m}$,
308 smaller than the classification of sand grains following the scheme proposed by Wentworth
309 (1922). Employing the additional median filter largely removed the occurrence of these small,
310 unexpected grains. Therefore, we suggest that the combination of a median filter with a non-
311 local means filter is effective in reducing over segmentation and identification of small,
312 unexpected features.

313 *The Influence of Grain Characteristics*

314 **Grain Size and Shape.**--- The observed lack of relationships between mean grain size
315 and both porosity and permeability (Figs. 3a and 3c) strongly suggests that grain size within
316 this suite of samples is not influential on the porosity-permeability relationship of the
317 respective pore structures. Nabawy (2014) presents a similar conclusion when examining the
318 influence of grain size on porosity and permeability in a series of idealised grain packs as well
319 as in high porosity sandstone samples. All but two of our samples are classified as very well-
320 well- or moderately-sorted (Folk 1980). Therefore, we suggest that future work should focus
321 on the relationship between grain size and porosity and permeability in a variety of
322 sandstones of different grain maturity, shape and facies to identify any factors which may
323 influence whether grain size presents a relationship with porosity or permeability.

324 In contrast, we show evidence that mean grain sphericity has a direct positive impact
325 on both porosity and permeability (Figs. 3b and 3d). Nabawy (2014) identifies a similar
326 relationship with the elongation (grain length/grain diameter) of grains within their sample
327 suite where less elongate grains contribute to greater porosity and permeabilities. Nabawy

This manuscript has not been peer reviewed and is a preprint only. It has been submitted to the Journal of Sedimentary Research.

328 (2014) uses elongation as a measure of grain anisotropy where a more elongate grain
329 indicates a greater degree of anisotropy. We can apply the same approach to grain sphericity,
330 where a less spherical grain indicates a greater degree of anisotropy. Following this paradigm,
331 we see that our results agree with those of Nabawy (2014), a greater degree of anisotropy of
332 the grains results in a reduction in both porosity and permeability.

333 We calculated a simple linear fit for the relationship between mean grain sphericity
334 and total porosity which is given by $\phi = 1.22 \phi_s - 0.42$. Nabawy (2014) proposes a
335 relationship between elongation, E and porosity using their sample suite where $\phi =$
336 $45.73 E^{-1} + 9.19$. This provides two parameters by which a porosity estimation may be
337 made based upon two different measures of grain anisotropy. Whilst Nabawy (2014) achieves
338 an elongation fit exhibiting a correlation coefficient of 0.92 we find our sphericity fit to have
339 a correlation coefficient of 0.65. We consider three separate sample suites from different
340 sedimentary facies, whilst Nabawy (2014) focusses on a single sample suite, which makes the
341 relationship between anisotropy and porosity less clear. Consequently, we suggest that
342 different depositional environments may have a more significant effect upon the
343 characteristics which influence the relationship between grain anisotropy and porosity, as
344 opposed to there being one consistent relationship being applicable across a wide variety of
345 sandstones. Further research is required to quantify the scale of this influence

346 We also investigated the control which the anisotropy of grains has on the geometry
347 of the pores themselves, finding that there is generally a positive relationship between grain
348 sphericity and pore diameter (Fig. 4). Our results agree with the relationship identified
349 between porosity and grain anisotropy, measured through elongation (Nabawy 2014). This
350 indicates that these two measures of grain anisotropy exhibit similar controls on porosity
351 which reflects directly in the geometry of the pore structures.

This manuscript has not been peer reviewed and is a preprint only. It has been submitted to the Journal of Sedimentary Research.

352 A suggested limitation of the relationship reported by Nabawy (2014) is that it may
353 depend on grain elongation occurring systematically along one axis which is common
354 throughout the sampled material. Such imbrication of grains according to their elongation
355 axes may result due to the flow of depositional currents and load pressure. Where such an
356 alignment is not clearly present, for example under depositional conditions where turbulent
357 flow dominates, these results imply that the detrimental impact on permeability would be far
358 more pronounced than any influence on the relationship with porosity. This conclusion
359 requires further testing using samples from varied depositional environments to eliminate
360 the effects of sorting and stratification.

361 We observe an apparent group of seven outliers when examining the relationship
362 between grain sphericity and permeability (Fig. 3d) which fall below the dominant trend. The
363 fact that this group of outliers are not apparent when comparing sphericity with porosity (Fig.
364 3b) strongly suggests that their rogue placement is due to a factor which inhibits fluid flow
365 but does not change the absolute porosity measurement. This may point towards a lack of
366 preferential orientation with regards to grain anisotropy within these particular samples.

367 Further investigation of the seven outliers found that there was no apparent common
368 characteristic amongst the outliers which could differentiate them from the remaining
369 samples. We investigated whether there was a relationship between these outliers and their
370 sample depth, sorting, porosity or permeability which might explain their occurrence. None
371 of these characteristics helped to explain the presence of the seven outliers. Furthermore, a
372 qualitative assessment of the μ CT images found nothing of significance which might allow for
373 the differentiation of this sample group such as presence of cement or other precipitates
374 which were not present in the main group of samples.

This manuscript has not been peer reviewed and is a preprint only. It has been submitted to the Journal of Sedimentary Research.

375 It might be expected that a lack of grain orientation would manifest throughout a
376 given geological unit, leading to surprise that the outlier group contains at least one sample
377 from each of the three studied formations. We suggest that the resulting texture may be
378 controlled by a different depositional process. Alternatively, the scale of the sample upon
379 which measurements were made could be considered not suitably representative for the
380 scale of the processes which cause variation in grain imbrication and alignment with regards
381 to anisotropy. Therefore, we suggest that future work should focus on identifying a suitable
382 representative elementary volume over which measures of grain anisotropy, such as
383 elongation and sphericity, can be representatively measured. Equally, identification and
384 implementation of a technique to measure and quantify alignment or imbrication of grains in
385 3D at the pore scale would be beneficial in providing greater context for relationships
386 between porosity and permeability with measures of grain anisotropy.

387 **Grain Influence on the Porosity-Permeability Relationship.**--- Despite the positive
388 relationship identified between mean grain sphericity and porosity and permeability (Figs. 3b
389 and d) we have found that the influence of grain characteristics is not beneficial to
390 constraining the porosity-permeability relationship in these sample suites (Fig. 6). This may
391 be a result of using a Kozeny-Carman fit equation which makes the assumption that grains are
392 spherical producing a simple pore structure (Rahrah et al. 2020). Bear (1972) describes how
393 this assumption arises from the transformation of the specific surface area term (Carman
394 1937) to a characteristic grain size term.

395 Inclusion of grain size in the paradigm of a Kozeny-Carman relationship defines the
396 diameter of the grain which is assumed to be spherical. However, we define grain size as the
397 greatest distance from one side of the grain to another or the calliper distance, which is
398 applicable to non-spherical grains. Therefore, as the sphericity of a given grain reduces, it

This manuscript has not been peer reviewed and is a preprint only. It has been submitted to the Journal of Sedimentary Research.

399 moves further from the Kozeny-Carman assumption which results in a poorer fit to samples
400 with a lower mean grain sphericity. We show that a lower sphericity results in a lower porosity
401 and permeability (Fig. 3) therefore, we would expect the Kozeny-Carman fit to be poorer at
402 lower porosities and permeabilities.

403 We show it to be the case that lower sphericity or greater grain anisotropy results in
404 a poorer agreement with a Kozeny-Carman based fit (Figs. 5 and 6). It can be observed that
405 below ca. 15% total porosity just one data point lies below the fit line whereas the remaining
406 data points lie consistently and significantly above the fit lines calculated using equation 6.
407 For example, sample PB12 has a low mean grain sphericity of 0.37 and a relatively low total
408 porosity of 9% and can be seen to plot above the black K-C fit line (Fig. 6). This strongly
409 suggests that the Kozeny-Carman style fit is not suitable for use with samples which possess
410 grains which show significantly low sphericities. Torskaya et al. (2014) investigate the effect
411 of grain shape on permeability and find that when using realistic grain shapes from μ CT
412 images that the K-C equation underestimates permeability by between 30 and 70%. When
413 using simplified and spherical grain shapes Torskaya et al. (2014) find that the K-C equation
414 fit was far more successful, supporting our conclusion that the K-C spherical grain assumption
415 is causing the poor quality fit. The K-C approach therefore, is not suitable for use with
416 materials where grains are significantly non-spherical.

417 As a result of this identified limitation, we propose that future work should look to
418 develop an alternative model which accounts for variation in grain sphericity within and
419 between different sandstone samples. In this study we have clearly shown that grain
420 sphericity exhibits a strong relationship with both porosity and permeability (Fig. 3),
421 highlighting the possible value in incorporating this grain characteristic in a porosity-
422 permeability model. A model which is still able to incorporate each influencing factor as

This manuscript has not been peer reviewed and is a preprint only. It has been submitted to the Journal of Sedimentary Research.

423 individual terms (as in equation 6) would be favourable to provide flexibility and the ability
424 for experimentation. Such a model could be tested against the simple and K-C models
425 presented in Figure 6 based upon RMSE.

426 Whilst many modified versions of the Kozeny-Carman equation have been proposed
427 and used (e.g., Le Gallo et al. 1998; MacQuarrie and Mayer 2005; Hommel et al. 2018), the
428 fundamental assumption of spherical grains and pores arranged as bundles of capillaries
429 remains. Alternatives to a K-C approach at the same scale have been used to describe
430 permeability such as the Fair-Hatch, Brinkman and Panda and Lake models, described and
431 summarised by Le Gallo et al. (1998) and MacQuarrie & Mayer (2005). Whilst some of these
432 approaches use grain size terms, they do not include terms which allow for direct inclusion of
433 grain shape or anisotropy.

434 A further consideration which would be highly beneficial to any future model would
435 be to account for the percolation threshold, a key phenomenon which makes effectively
436 characterising the porosity-permeability relationship difficult over a range of porosities.
437 Thomson, et al. (2020b) and Payton et al. (2021) show the percolation threshold for full
438 connectivity to be at ca. 8 - 15% total porosity, whilst Mavko & Nur (1997) and Rahrah et al.
439 (2020) show the value of incorporating the percolation threshold into a K-C style fit.
440 Consideration of the percolation threshold alongside variable grain sphericity would surely be
441 an effective approach to best describe the porosity-permeability relationship.

442

443

CONCLUSIONS

444 In this work we made a comparison of two similar grain segmentation techniques,
445 using marker-based watershed algorithms, for reliable and accurate grain boundary
446 identification across our sample suites. We found that using a median filter in addition to a

This manuscript has not been peer reviewed and is a preprint only. It has been submitted to the Journal of Sedimentary Research.

447 non-local means (NLM) filter prior to segmentation resulted in superior grain separation as
448 opposed to using a NLM filter alone. This appeared to be due to the ability of the median filter
449 to preserve and enhance the grain edges during denoising, reducing oversegmentation. The
450 low computational cost and high speed at which this technique can be applied makes this a
451 suitable option for segmentation of sandstone materials such as those investigated here.

452 We have used digital image analysis techniques on μ CT images of three different suites
453 of sandstone samples to investigate the impact of grain characteristics on the porosity-
454 permeability relationship. We have shown that in this collection of samples the porosity-
455 permeability relationship is not better constrained when including grain shape and size
456 parameters in a Kozeny-Carman type fit equation. This is the case despite identification of a
457 strong positive relationship between grain sphericity and both porosity and permeability. We
458 found no such relationship with grain size. Therefore, we found a porosity-permeability
459 relationship best described by $K = 10^{5.54} \phi^{3.7}$.

460 We determine that the need to assume that grains are spherical when working in a
461 Kozeny-Carman paradigm is severely limiting to identifying an effective porosity-permeability
462 relationship. Future work should focus on incorporating a grain sphericity term in a model
463 which effectively handles non-spherical and non-uniform grains. Of added benefit would be
464 consideration of the percolation threshold in producing a model capable of constraining the
465 porosity-permeability relationship over a range of porosities in sandstones.

466 Finally, consideration of grain sphericity as a measure of 3D grain shape anisotropy
467 revealed a relationship of decreasing anisotropy resulting in greater porosity and
468 permeability, in agreement with 2D measures of grain anisotropy. We found total porosity to
469 vary with grain sphericity according to $\phi = 1.22\phi - 0.42$, offering an additional indirect
470 method of predicting porosity. A group of outliers are identified, vertically displaced below

This manuscript has not been peer reviewed and is a preprint only. It has been submitted to the Journal of Sedimentary Research.

471 the main trend of the sphericity-permeability data. We suggest that this may be due to a lack
472 of grain orientation with regards to sphericity in these samples, inhibiting the permeability
473 only as the same occurrence is not observed so strongly in the case of porosity.

474

475

REFERENCE LIST

476 Barraud J., 2006, The use of watershed segmentation and GIS software for textural analysis
477 of thin sections: *Journal of Volcanology and Geothermal Research*, v. 154, p. 17–33.

478 Bear J., 1972, *Dynamics of fluids in porous media*. American Elsevier.

479 Berg C.F., 2014, Permeability Description by Characteristic Length, Tortuosity, Constriction
480 and Porosity: *Transport In Porous Media*, v. 103, p. 381–400.

481 Beucher S. and Meyer F., 2018, The Morphological Approach to Segmentation: The
482 Watershed Transformation, *in Mathematical Morphology in Image Processing*, 1st edn,
483 CRC Press, p. 433–481.

484 Blunt M.J., Bijeljic B., Dong H., Gharbi O., Iglauer S., Mostaghimi P., Paluszny A. and Pentland
485 C., 2013, Pore-scale imaging and modelling: *Advances In Water Resources*: v. 51, p.
486 197–216.

487 Buades A., Coll B. and Morel J-M., 2008, Nonlocal Image and Movie Denoising: *International
488 Journal of Computer Vision*, v.76, p. 123–139.

489 Buades A., Coll B. and Morel J-M., 2010, Image Denoising Methods. A New Nonlocal
490 Principle: *SIAM Review*, v. 52, p. 113–147.

491 Bultreys T., Van Hoorebeke L. and Cnudde V., 2015, Multi-scale, micro-computed
492 tomography-based pore network models to simulate drainage in heterogeneous rocks:
493 *Advances In Water Resources*, v. 78, p. 36–49.

494 Campbell A., Murray P., Yakushina E., Marshall, S. and Ion W., 2018, New methods for

This manuscript has not been peer reviewed and is a preprint only. It has been submitted to the Journal of Sedimentary Research.

- 495 automatic quantification of microstructural features using digital image processing:
496 *Materials and Design*, v. 141, p. 395–406.
- 497 Carman P.G., 1937, Fluid flow through granular beds: *Transaction of the Institution of*
498 *Chemical Engineers*, v.15, p. 150–156.
- 499 Cristoforetti A., Faes L., Ravelli F., Centonze M., Del Greco M., Antolini R. and Nollo G., 2008,
500 Isolation of the left atrial surface from cardiac multi-detector CT images based on
501 marker controlled watershed segmentation: *Medical Engineering and Physics*, v. 30, p.
502 48–58.
- 503 de Lima O.A. and Niwas, S., 2000, Estimation of hydraulic parameters of shaly sandstone
504 aquifers from geoelectrical measurements: *Journal of Hydrology*, v. 235, p. 12–26.
- 505 Fei W., Narsilio G.A. and Disfani M.M., 2019, Impact of three-dimensional sphericity and
506 roundness on heat transfer in granular materials: *Powder Technology*, v. 355, p. 770–
507 781.
- 508 Fei W. and Narsilio G.A., 2020, Impact of Three-Dimensional Sphericity and Roundness on
509 Coordination Number: *Journal of Geotechnical and Geoenvironmental Engineering*, v.
510 146, no. 06020025.
- 511 Folk R.L., 1980, *Petrology of sedimentary rocks*. Hemphill Publishing Company.
- 512 Furat O., Wang M., Neumann M., Petrich L., Weber M., Krill C.E. and Schmidt V., 2019,
513 Machine Learning Techniques for the Segmentation of Tomographic Image Data of
514 Functional Materials. *Frontiers in Materials*, v. 6, no. 145.
- 515 Hommel J., Coltman E. and Class H., 2018, Porosity–Permeability Relations for Evolving Pore
516 Space: A Review with a Focus on (Bio-)geochemically Altered Porous Media: *Transport*
517 *In Porous Media*, v. 124, p. 589–629.
- 518 Huang H., Li X. and Chen C., 2018, Individual Tree Crown Detection and Delineation From

This manuscript has not been peer reviewed and is a preprint only. It has been submitted to the Journal of Sedimentary Research.

- 519 Very-High-Resolution UAV Images Based on Bias Field and Marker-Controlled
520 Watershed Segmentation Algorithms: IEEE Journal of Selected Topics in Applied Earth
521 Observations and Remote Sensing, v. 11, p. 2253–2262.
- 522 Kong D. and Fonseca J., 2018, Quantification of the morphology of shelly carbonate sands
523 using 3D images: Géotechnique, v. 68, p. 249–261.
- 524 Kozeny J., 1927, Über kapillare Leitung des Wassers im Boden: Sitzungsber Akad Wiss Wien,
525 v. 136, p. 271–306.
- 526 Le Gallo Y., Bildstein O. and Brosse E., 1998, Coupled reaction-flow modeling of diagenetic
527 changes in reservoir permeability, porosity and mineral compositions: Journal of
528 Hydrology, v. 209, p. 366–388.
- 529 Legland D., Arganda-Carreras I. and Andrey P., 2016, MorphoLibJ: integrated library and
530 plugins for mathematical morphology with ImageJ: Bioinformatics, v. 32, p. 3532–3543.
- 531 Leonti A., Fonseca J., Valova I., Beemer R., Cannistraro D., Pilskaln C., DeFlorio D. and Kelly
532 G., 2020, Optimized 3D Segmentation Algorithm for Shelly Sand Images: Proceedings of
533 the 6th World Congress on Electrical Engineering and Computer Systems and Science,
534 p. CIST 107.
- 535 MacQuarrie K.T.B. and Mayer K.U., 2005, Reactive transport modeling in fractured rock: A
536 state-of-the-science review: Earth-Science Reviews, v. 72, p. 189–227.
- 537 Mavko G. and Nur A., 1997, The effect of a percolation threshold in the Kozeny-Carman
538 relation: GEOPHYSICS, v. 62, p. 1480–1482.
- 539 Nabawy B.S., 2014, Estimating porosity and permeability using Digital Image Analysis (DIA)
540 technique for highly porous sandstones: Arabian Journal of Geosciences, v. 7, p. 889–
541 898.
- 542 Ollion J., Cochennec J., Loll F., Escudé, C. and Boudier T., 2013, TANGO: a generic tool for

This manuscript has not been peer reviewed and is a preprint only. It has been submitted to the Journal of Sedimentary Research.

- 543 high-throughput 3D image analysis for studying nuclear organization: *Bioinformatics*, v.
544 29, p. 1840–1841.
- 545 Otsu N., 1979, A Threshold Selection Method from Gray-Level Histograms: *IEEE Transactions*
546 *on Systems, Man and Cybernetics*, v. 9, p. 62–66.
- 547 Payton R.L., Fellgett M., Clark B.L., Chiarella D., Kingdon A. and Hier-Majumder S., 2021,
548 Pore-scale assessment of subsurface carbon storage potential: implications for the UK
549 Geoenergy Observatories project: *Petroleum Geoscience*, v. 27, no. petgeo2020-092.
- 550 Rahrah M., Lopez-Peña L.A., Vermolen F. and Meulenbroek B., 2020, Network-inspired
551 versus Kozeny–Carman based permeability-porosity relations applied to Biot’s
552 poroelasticity model: *Journal of Mathematics in Industry*, v. 10, p. 19.
- 553 Schäfer A. and Teyssen T., 1987, Size, shape and orientation of grains in sands and
554 sandstones—image analysis applied to rock thin-sections: *Sedimentary Geology*, v. 52,
555 p. 251–271.
- 556 Schindelin J., Arganda-Carreras I., Frise E., Kaynig V., Longair M., Pietzsch T., Preibisch S.,
557 Rueden C., Saalfeld S., Schmid B., Tinevez J.-Y., White D.J., Hartenstein V., Eliceiri K.,
558 Tomancak P., and Cardona A., 2012, Fiji: an open-source platform for biological-image
559 analysis: *Nature Methods*, v. 9, p. 676–682.
- 560 Shi Y., and Yan W.M., 2015, Segmentation of irregular porous particles of various sizes from
561 X-ray microfocus computer tomography images using a novel adaptive watershed
562 approach: *Géotechnique Letters*, v. 5, p. 299–305.
- 563 Suhr B., Marschnig S. and Six K., 2018, Comparison of two different types of railway ballast
564 in compression and direct shear tests: experimental results and DEM model validation:
565 *Granular Matter*, v. 20, p.70.
- 566 Sun Q., Zheng J. and Li C., 2019, Improved watershed analysis for segmenting contacting

This manuscript has not been peer reviewed and is a preprint only. It has been submitted to the Journal of Sedimentary Research.

- 567 particles of coarse granular soils in volumetric images: *Powder Technology*, v. 356, p.
568 295–303.
- 569 Thomson P-R., Aituar-Zhakupova A. and Hier-Majumder S., 2018, Image Segmentation and
570 Analysis of Pore Network Geometry in Two Natural Sandstones: *Frontier in Earth*
571 *Sciences*, v. 6, no. 58.
- 572 Thomson P-R., Hazel A. and Hier-Majumder S., 2019, The Influence of Microporous Cements
573 on the Pore Network Geometry of Natural Sedimentary Rocks: *Frontiers in Earth*
574 *Sciences*, v. 7, no. 48.
- 575 Thomson P-R., Ellis R., Chiarella D. and Hier-Majumder S., 2020a, Microstructural Analysis
576 From X-Ray CT Images of the Brae Formation Sandstone, North Sea: *Frontiers in Earth*
577 *Sciences*, v. 8, no. 246.
- 578 Thomson P-R., Jefferd M., Clark B.L., Chiarella D., Mitchell T.M. and Hier-Majumder S.,
579 2020b, Pore network analysis of Brae Formation sandstone, North Sea: *Marine and*
580 *Petroleum Geology*, v. 122, no. 104614.
- 581 Torskaya T., Shabro V., Torres-Verdín C., Salazar-Tio, R. and Revil, A., 2014, Grain Shape
582 Effects on Permeability, Formation Factor, and Capillary Pressure from Pore-Scale
583 Modeling: *Transport in Porous Media*, v. 102, p. 71–90.
- 584 Urumovic K. and Urumovic Sr. K., 2014, The effective porosity and grain size relations in
585 permeability functions: *Hydrology and Earth System Sciences Discussions*, v. 11, p.
586 6675–6714.
- 587 Veta M., Huisman A., Viergever M.A., van Diest P.J. and Pluim J.P.W., 2011, Marker-
588 controlled watershed segmentation of nuclei in H&E stained breast cancer biopsy
589 images: 2011 IEEE International Symposium on Biomedical Imaging: From Nano to
590 Macro, p. 618–621.

This manuscript has not been peer reviewed and is a preprint only. It has been submitted to the Journal of Sedimentary Research.

591 Keller W.D., 1945, Size Distribution of Sand in Some Dunes, Beaches, and Sandstones: AAPG
592 Bulletin, v. 29, p. 215–221.

593 Wang J-J., Zhang H-P., Deng D-P. and Liu M-W., 2013, Effects of mudstone particle content
594 on compaction behavior and particle crushing of a crushed sandstone–mudstone
595 particle mixture: Engineering Geology, v. 167, p. 1–5.

596 Wentworth C.K., 1922, A Scale of Grade and Class Terms for Clastic Sediments: Journal of
597 Geology, v. 30, p. 377–392.

598 Xue Y., Zhao J. and Zhang M., 2021, A Watershed-Segmentation-Based Improved Algorithm
599 for Extracting Cultivated Land Boundaries: Remote Sensing, v. 13, p. 939.

600

601

CONFLICT OF INTEREST STATEMENT

602 The authors declare that the research was conducted in the absence of any
603 commercial or financial relationships that could be construed as a potential conflict of
604 interest.

605

606

AUTHOR CONTRIBUTIONS

607 Conceptualisation: Ryan L. Payton, Domenico Chiarella; Methodology: Ryan L. Payton;
608 Formal analysis and investigation: Ryan L. Payton; Writing - original draft preparation: Ryan L.
609 Payton; Writing - review and editing: Ryan L. Payton, Domenico Chiarella, Andrew Kingdon;
610 Supervision: Domenico Chiarella, Andrew Kingdon.

611

612

FUNDING

This manuscript has not been peer reviewed and is a preprint only. It has been submitted to the Journal of Sedimentary Research.

613 RLP acknowledges support from a NERC DTP studentship (grant number
614 NE/L002485/1) as well as further financial support through a CASE partnership with the British
615 Geological Survey as part of their British University Funding Initiative.

616

617

ACKNOWLEDGEMENTS

618 The authors would like to thank Paul-Ross Thomson for his useful input regarding the
619 methodology and Frank Lehane (RHUL) for his computational support throughout the project.
620 This manuscript was published with the permission of the Executive Director of the British
621 Geological Survey.

622

623

DATA AVAILABILITY STATEMENT

624 The μ CT images used in this article are available from a variety of sources. Images of
625 the Wilmslow Sandstone Fm. for samples with a SF prefix are available from Payton et al.
626 (2021). Images of the Brae Fm. Sandstone for samples with BFS prefix are not publicly
627 available and must be requested from Thomson, et al. (2020b). Images of the Minard
628 Formation Sandstone from the Porcupine Basin for samples with a PB prefix are available from
629 the Royal Holloway, University of London Figshare Repository,
630 <https://figshare.com/s/a3c53f2b89fb3d655f6a>.

631

632

FIGURE CAPTIONS

633 **Figure 1.** Schematic diagram showing the typical steps in grain identification using a
634 watershed technique on CT images.

635 **Figure 2.** Isolated collection of grains (white) and single grain (orange) shown in 3D
636 from sample SF696. The saw-tooth or staircase pattern is highlighted which arises from the

This manuscript has not been peer reviewed and is a preprint only. It has been submitted to the Journal of Sedimentary Research.

637 voxelised images. This can lead to overestimation of surface area and impact the
638 subsequent sphericity measurements.

639 **Figure 3.** Relationship between mean grain size, mean grain sphericity and total
640 porosity and permeability. A generally positive relationship with porosity and permeability
641 can be observed in the case of mean grain sphericity but no such relationship is present with
642 mean grain size. A region of outliers is identified by a dashed line in **(d)** with the same data
643 points also identified in **(b)**.

644 **Figure 4.** Relationship between mean grain sphericity and mean connected pore
645 diameter for each of the three sample suites. It is apparent that there is a generally positive
646 relationship between the two parameters.

647 **Figure 5.** Range of calculated fit configurations to the porosity-permeability
648 relationship which incorporate grain characteristics using a Kozeny-Carman based
649 relationship. The table to the right qualitatively describes the difference between each fit
650 line whilst the respective equations are displayed in the plot legend.

651 **Figure 6.** Calculated fits to the porosity-permeability relationship. The root mean
652 square error (RMSE) values are reported for each fit, showing that the better fit is the
653 simpler one in green. The green fit excludes any measured grain characteristics whereas the
654 black fit does not.

655 **Figure 7.** Comparison of two different filtering techniques' effect on the watershed
656 algorithm in a single slice of sample PB10. Four different locations have been highlighted for
657 comparison on an image which has undergone non-local means (NLM) filtering only.
658 Annotated squares show the result of watershed grain segmentation following only NLM
659 (Thomson et al. 2020a) and NLM with a median filter (Fei and Narsilio 2020). Each grain can
660 be identified by a different colour however, due to the number of grains, colours have been

This manuscript has not been peer reviewed and is a preprint only. It has been submitted to the Journal of Sedimentary Research.

661 reused and instead the black grain boundaries split different grains of the same
 662 colour. In each annotation an example of over-segmentation is observed in the case of using
 663 NLM filtering only when compared to what we might expect from the CT image. The outer
 664 scale bar applies to all annotations.

665

666 **Table 1.** Summary of the sampled materials analysed in this study.

Sampling Location	Well ID	Sample ID	Depth (m)	Geology	
Porcupine Basin, N. Atlantic	26/28-1	PB01 PB02 PB03 PB05	2271 2256.4 2420 2420.48	Minard Formation	Renard Member
	26/28-2	PB06 PB07 PB08 PB10 PB11 PB12	2117 2118 2116.8 2118.6 2119.15 2119.85		Dooneragh Member
Sellafield, UK*	SFBH13B	SF696 SF697 SF698 SF699 SF700 SF701 SF702	63.8 76.1 96.98 126.27 144.03 172.16 181.39	Wilmslow Sandstone Formation	
North Sea, UK**	16/7b-20	BFS1 BFS2 BFS4	4040.1 4041.35 4045.13	Brae Formation Sandstone	
	16/7b-23	BFS5 BFS8	4061 4063.75		

667

668 *Payton et al. (2021), **Thomson et al. (2020b).

669

670

671

672 **Table 2.** Grain-based measurements made for each sample.
673

Sample	Sorting (ϕ)	Mean Grain Size (μm)	Mean Grain Sphericity
PB01	0.63	242	0.45
PB02	0.61	298	0.43
PB03	0.44	112	0.47
PB05	0.45	297	0.47
PB06	0.55	198	0.46
PB07	0.45	92	0.44
PB08	0.42	168	0.48
PB10	0.49	120	0.45
PB11	0.78	223	0.40
PB12	0.56	117	0.37
SF696*	0.61	203	0.49
SF697*	0.54	205	0.46
SF698*	0.64	204	0.52
SF699*	0.50	257	0.53
SF700*	0.51	230	0.46
SF701*	0.51	179	0.50
SF702*	0.52	247	0.45
BFS1**	0.61	135	0.44
BFS2**	0.75	262	0.43
BFS4**	0.69	158	0.44
BFS5**	0.53	421	0.43
BFS8**	0.44	108	0.46

674
675 *Payton et al. (2021), **Thomson et al. (2020b).
676

677

678

679

680

681

682

683

684

685
686

Table 3. Porosity and permeability measurements made for each sample.

Sample	Total Porosity (%)	Connected Porosity (%)	Permeability (mD)
PB01	20.4	20.3	1070
PB02	10.5	9.8	147
PB03	12.2	10.2	99
PB05	11.2	4.9	37
PB06	6.7	5.2	21
PB07	9.6	8.9	46
PB08	13.6	13.3	123
PB10	12.9	9.7	237
PB11	14.1	13.6	36
PB12	9	6.9	18
SF696*	20.7	20.4	1760
SF697*	20.7	20.3	620
SF698*	22.9	22.7	3190
SF699*	26.4	26.3	6040
SF700*	17.0	16.6	360
SF701*	24.3	24.1	1420
SF702*	9.77	8.89	40
BFS1**	7.2	5.8	91
BFS2**	7.1	5.7	86
BFS4**	9.6	9.1	104
BFS5**	7.8	5.1	6.7
BFS8**	15.2	14.8	795

687
688

*Payton et al. (2021), **Thomson et al. (2020b).